Renewable Energy 187 (2022) 440–449

Contents lists available at ScienceDirect

Renewable Energy

journal homepage: www.elsevier.com/locate/renene

Impacts of transmembrane pH gradient on nanofluidic salinity gradient energy conversion

Xi Chen , Zuoqing Luo , Rui Long *, Zhichun Liu , Wei Liu

School of Energy and Power Engineering, Huazhong University of Science and Technology, Wuhan, 430074, PR China

ARTICLE INFO

Article history:
Received 16 September 2021
Received in revised form
12 January 2022
Accepted 24 January 2022
Available online 29 January 2022

Keywords:
Reverse electrodialysis
Nanofluidics
pH regulation
Salinity gradient power

ABSTRACT

Solution pH can impact the nanochannel surface charge density, thus, to regulate the transmembrane ion transportation. Here, the performance of nanofluidic salinity gradient energy conversion is investigated, where the solution pH at the high/low concentration side varies separately, rendering asymmetric pH configurations. Results reveal that the solution pH at the low concentration side (pH_L) exhibits a significant impact on the salinity gradient energy conversion. When pH_L < Isoelectric Point (IEP), the energy conversion indicators are most stable under various solution pH at the high concentration side (pH_H). The surface charge density of the nanochannel at the low concentration end determines the transmembrane ion transportation characteristics, dominating the energy conversion performance. The energy conversion performance via nanochannels of different lengths under asymmetric pH configurations is also studied. There exists optimal nanochannel length corresponding to the maximum electric power, which differs under various pH configurations. For longer nanochannels, the ion concentration polarization effect is weakened, allowing for a more effective energy extraction performance via pH-adjusted salinity gradients. At the length of 2000 nm, the electric power and energy conversion efficiency under the co-direction configuration is 78% and 97.9%, respectively, larger than those under the reverse direction configuration.

1. Introduction

Excessive utilization of traditional fossil energy sources induces severe environmental problems, such as haze, global warming, and the greenhouse effect [1,2]. Exploiting and utilizing new green and renewable energy resources is on the table [3–5]. Salinity gradient energy is abundant and widely distributed on the earth [6,7], which can be converted to electricity by various technologies, such as pressure retarded osmosis (PRO) and reverse electrodialysis (RED) [8–10]. The latter has received increasing attention due to its high reliability and lower requirements [11,12]. Membrane-based RED can be combined with microbial electrochemical systems [13,14] or desalination, which can provide highly concentrated brines to enhance the performance of RED [15,16]. However, the unsatisfied low power density of the traditional RED stacks via ion exchange membranes (IEM) hinders its widely commercial application {Mokhtar, 2021 #2335} [17]. The pore size of traditional ion exchange membranes is rather small, which results in low osmotic current and power extracted [18]. Charged nanochannels that repel co-ions and attract counter ions, exhibiting ionic selectivity for counter ions, can function as the IEMs, paving an alternative way to improve the energy conversion performance in the RED process due to their large pore size that induces higher ionic flux [18].

Many efforts have been devoted to augmenting the nanofluidic energy conversion performance via charged nanochannels. Siria et al. [19]employed boron nitride nanochannels to obtain huge currents that exceeded by two orders of magnitude those obtained using conventional methods. Kim et al. [20]studied the power generation from KCL solution in silica nanochannels and measured the highest power density of 7.7 W/m^2, while the optimum efficiency was 31%. Kang et al. [21]investigated the RED phenomenon in anodized aluminum and obtained an energy density of 9.9 W/m^2. Feng et al. [22]developed a novel MOS_2 material and obtained a power of 10^6 W/m^2 using a monolayer MOS_2 film under the potassium chloride salt gradient. Gao et al. [23]obtained a power density of 3.46 W/m^2 by mixing artificial seawater and river water through 7 nm mesoporous carbon and 80 nm microporous alumina.

* Corresponding author.
E-mail address: r_long@hust.edu.cn (R. Long).

https://doi.org/10.1016/j.renene.2022.01.099
0960-1481/

In the nanochannels, the ionic current rectification (ICR) phenomenon has also been studied [24]. The impacts of geometry as well as membrane material and concentration have been investigated. Hsu et al. [25]investigated the effect of electroosmotic flow on the rectification behaviors of ionic currents in conical nanochannels, and found that the relative magnitude of the rectification factor for various salts depends on the applied electromotive bias level if EOF is not neglected. Hsu et al. [26]revealed that if the salt concentration is high enough or the cone angle is large enough, the magnitude of rectification rate will be reversed between different types of salts at larger applied voltage bias. The influences of pore size, electrolyte concentration and half cone angle on the ICR of glass nanochannel membranes were investigated by Kubeil et al. [27].

The performance of the nanofluidic energy conversion system is affected by nanochannel geometry, surface charge density, ion species, temperature, and pH, and higher nanochannel efficiency can be obtained by changing the combination of various influencing factors [28–34]. Among these influencing factors, temperature and pH on both sides of the nanochannel are relatively more feasible to change and can therefore be chosen to regulate the performance of the nanofluidic salinity gradient energy harvesting. Ma et al. [35]developed an analytical model of surface charge properties and ionic currents/inductance in pH-regulated nanochannels and found significant overlapping effects of EDL at small nanochannel heights, low salt concentrations, and low to medium pH values. Tseng et al. [36]revealed that salinity gradient power is strongly dependent on the effect of temperature, and higher power corresponds to higher temperature, while the efficiency of the nanochannel does not vary much with temperature. Long et al. [18,37,38] investigated the salinity gradient power at asymmetric temperatures and found that the counter-diffusion temperature gradient can reduce the ion concentration polarization effect at the low concentration end and therefore improve the ion selectivity of nanochannels and increase the power. Peng et al. [39]found that the polarity of the conical nanochannel rectifier can be changed by varying the acidity and alkalinity at both ends of the nanochannel. Mai et al. [40]found that the power generation increases as the pH increases from 5 to 10, but decreases when the pH increases further to 11 due to the strong ICP effect. Hsu et al. [41]investigated pH-adjusted conical nanochannels and found that the farther the pH deviates from neutral leads to an increase in surface charge density and therefore to an increase in the power generated. The effect of H^+ and OH^- generation needs to be considered in significantly acidic or alkaline environments. Yeh et al. [42]discussed pH-dependent nanofluid salinity gradient power and proposed anomalous dependence of system power on charge density, suggesting that higher surface charge density corresponding to nanochannels will not necessarily have higher power. These studies proved the positive effect of pH regulation on optimizing the power density of salinity gradient energy harvesting. In addition, Long et al. [5] proposed three synergy angles to describe the synergy relations between the ion diffusion and the electrostatic migration driven forces.

However, previous studies concerning the impacts of pH on the salinity gradient energy harvesting have only focused on the specific condition where the solution pH at both ends of the nanochannel is kept identical and varies simultaneously. The performance of nanofluidic salinity gradient energy conversion under asymmetric pH configurations (the solution pH differs from each other at the nanochannel side) has never been reported. Here, the impacts of transmembrane pH gradients on nanofluidic salinity gradient energy conversion are systematically investigated. The solution pH at the high concentration and low concentration varies separately, rendering asymmetric pH configurations, and establishing transmembrane pH gradients. The osmotic current, membrane potential, maximum output electric power, and maximum power efficiency under the asymmetric pH configurations are investigated. The energy conversion performance via nanochannels of different lengths under asymmetric pH configurations is also researched. The underlining mechanism is revealed. This study may provide new insights into the pH-regulation nanofluidic salinity-gradient energy harvesting.

2. System description

Appropriate nanopore size can improve the EDL overlap degree and ion selectivity. Guo et al. [43] suggested that 10–50 nm nanopores can optimize efficiency and power density. As shown in Fig. 1, in the present study, the salinity gradient energy conversion performance in a cylindrical nanochannel with a radius of $Ra = 10$ nm at varied channel lengths is investigated. The radius of the reservoir is set to 1000 nm to reduce the impact of reservoir size. The nanopore connects two reservoirs filled with KCl solution, whose concentration is fixed at 1000 mM or 1 mM at either side, rendering a transmembrane concentration ratio of 1000:1. The pH on either side varies from 3 to 9, respectively. Induced by the solution pH, the surface charge density in the nanochannel is spatially distributed, which can be calculated as follows [42]:

$$\sigma_W = -\left(10^{18} e N_{\text{total}}\right) \times \left\{ \frac{10^{-pK_A} - 10^{-pK_B} H^+ \left[H^+\right]\left[H^+\right]_S)^2}{10^{-pK_A} + 10^{-pK_B} H^+ \left[H^+\right]\left[H^+\right]_S)^2 + \left[H^+\right]_S} \right\} \tag{1}$$

where $pK_A = 2.302 pK_B = 9.46$ at T = 290 K for the polyethylene terephthalate (PET) nanochannel [44]. Therefore, the isoelectric point (IEP) is about 6.

The Poisson-Nernst-Planck equations and Navier-Stokes equations are employed to illustrate transmembrane ion transportation and flow characteristics [18,45,46].

$$-\nabla \cdot (\varepsilon \nabla \varphi) = F \sum_{i=1}^{4} z_i c_i \tag{2}$$

$$\nabla \cdot \boldsymbol{J}_i = 0, \bullet \text{where} \boldsymbol{J}_i = c_i \boldsymbol{u} - D_i \nabla c_i - \frac{D_i z_i F c_i}{RT} \nabla \varphi \tag{3}$$

$$-\nabla p + \nabla \cdot \left(\mu \nabla \boldsymbol{u}\right) - F \sum_{i=1}^{4} z_i c_i \nabla \varphi = 0 \tag{4}$$

$$\nabla \cdot \boldsymbol{u} = 0 \tag{5}$$

where φ is the electrical potential. $\boldsymbol{J}_i$, c_i, D_i and z_i denotes the ionic flux, concentration, diffusivity, and valence of the ith ($i = 1$–4 for K^+, Cl^-, H^+ and OH^-) ionic species, respectively. F is the Faraday constant. R is the universal gas constant. ε, p, and $\boldsymbol{u}$ are the permittivity, pressure, and velocity of the solution, respectively. The diffusive coefficient D_i for each ionic species is calculated by the Nernst-Haskell equation: [38].

$$D_i = \frac{RT}{F^2}\left[\frac{1/|z_i|}{1/\lambda_i^0}\right] \tag{6}$$

where λ_i^0 is the limiting conductance of the ith ionic species. At the

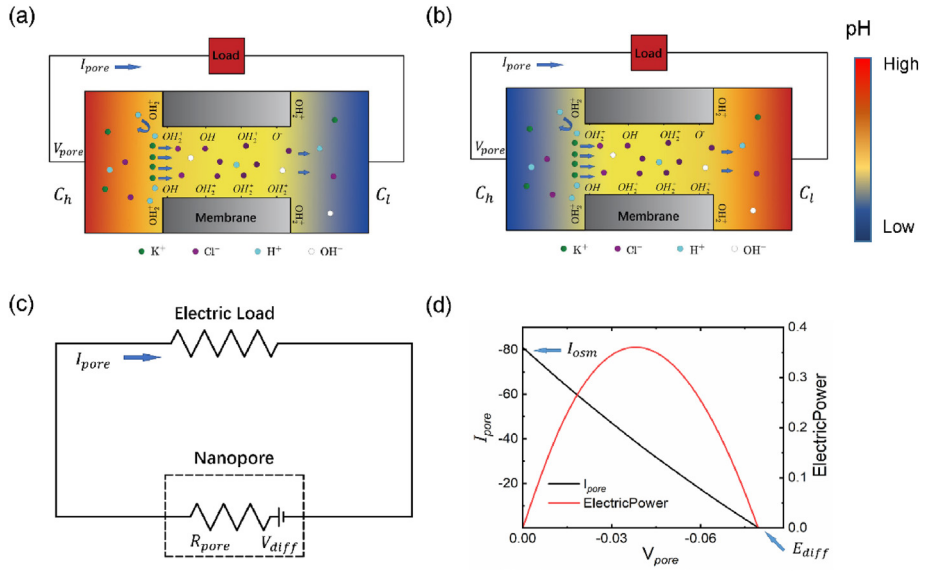

Fig. 1. (a, b) Schematic diagram of the nanofluidic energy conversion system under the concentration gradient and pH gradient. (c) Schematic diagram of the equivalent circuit diagram. (d) Relationship between nanochannel osmotic current and output electric power, and the calculation of I_{osm} and E_{diff}.

temperature of 290K, $\lambda_1^0 =$ 62.1104 $\lambda_2^0 =$ 64.1118, $\lambda_3^0 =$ 309.9565 and $\lambda_4^0 =$ 171.0202.

Equations (2)–(5) can be solved with proper boundary conditions. The boundary conditions are listed below: [18].

$$-\varepsilon \mathbf{n}\cdot\nabla\varphi = 0 \cdot \text{on} \cdot \Omega_r \text{and} \cdot \Lambda_j \tag{7}$$

$$-\varepsilon \mathbf{n}\cdot\nabla\varphi = \sigma \cdot \text{on} \cdot \Omega_n \tag{8}$$

$$\mathbf{n}\cdot\mathbf{J}_i = 0 \cdot \text{on} \cdot \Omega_r \text{and} \cdot \Lambda_j \tag{9}$$

where Ω_n、 Ω_r、 Λ_j denote the boundaries at the channel surface, the inner surface of the reservoir, and the reservoir ends, respectively.

The ionic current can be calculated by the following equation:

$$I = \int_A F\left(\sum_i^4 z_i J_i\right)\cdot n d\Lambda \tag{10}$$

when no applied voltage is applied on both sides of the channel, the osmotic current I_{osm} can be calculated using $I_{\text{osm}} = I_+ + I_-$, where I_+ and I_- are the currents contributed by cations and anions, respectively. The ionic selectivity can be characterized by ion transference number t_+, which is defined as the ratio of the anions passing through the nanopore:

$$t_+ = \frac{I_+}{I_+ + |I_-|} \tag{11}$$

As shown in Fig. 1(d), the membrane potential (V_{diff}) and osmotic current have a good linear relationship [37], the open-circuit voltage can be obtained by fitting the current with different applied voltages. The maximum output power can be obtained from Ohm's law as

$$P_{\max} = \left(V_{\text{diff}} \times I_{osm}\right) \Big/ 4 \tag{12}$$

The efficiency at maximum power is given by

$$\eta_{\text{max power}} = \frac{(2t_+ - 1)^2}{2} \tag{13}$$

3. Results and discussion

3.1. Model validation

Numerical simulation for the nanofluidic salinity gradient conversion process is conducted via the commercial Multiphysics software COMSOL. Quadrilateral meshes are employed and are finned near the charged membrane wall surface. The grid independence was verified using the grids numbers of 324000, 564000, 870000, 1260000, respectively. As shown in Table 1, the grid with the number 870000 was selected due to its high accuracy and low consumption. As shown in Fig. 2, the experimental data [19] have good consistency with the simulation results obtained by the model considering the impacts of the H^+ and the OH^- included.

3.2. Impacts of the solution pH at the high concentration side

Here the impacts of the solution pH at the high concentration side on the energy conversion performance are systematically investigated. The pH at the high concentration side of the nanochannel varies from pH = 3 to pH = 9 with the pH on the low concentration side fixed at different values. The pH at the low concentration side is denoted as pH_L and that at the high concentration side is denoted as pH_H. The relation of the cation transference number and pH_H under various pH_L is shown in Fig. 3. When pH_L < IEP (pH_L = 3), the cation transference number is almost not affected by pH_H. When pH_L = IEP (pH = 6), the ion selectivity gradually decreases with the change of pH_L and the ion

Table 1
Mesh independence analysis.

Mesh number	324000	564000	870000	1260000
Osmotic current (nA)	−79.29	−80.38	−80.80	−80.82

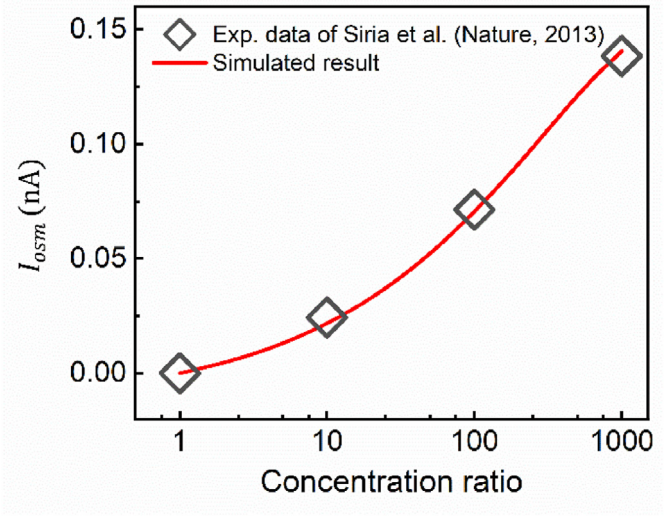

Fig. 2. Comparison between the experimental data obtained by Siria et al. [19] in a boron nitride nanotube and the present simulated result with radius Ra = 40 nm and length La = 1000 nm at pH = 5.5.

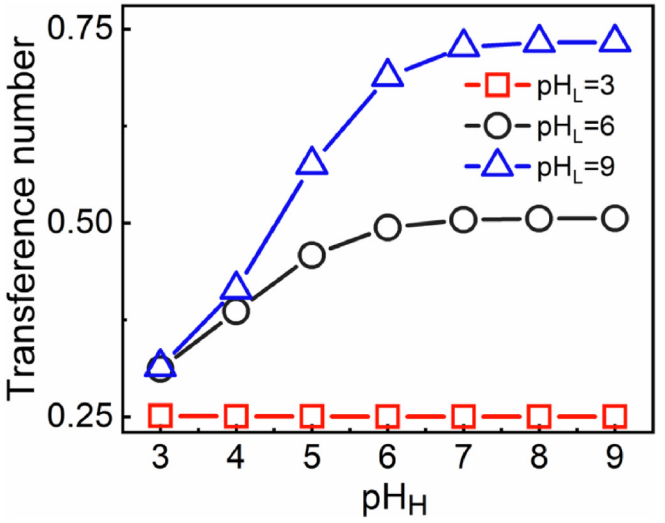

Fig. 3. The relation of the cation transference number and pH_H under various pH_L.

selectivity approaches 0 after pH_H>=IEP. The phenomenon is different when pH_L > IEP. The ion selectivity decreases and then increases as the pH_H increases and remains high and stable at larger pH_H.

To analyze the ion selectivity of the nanochannel, Long et al. [5] introduced the concept of synergistic angle:

$$\alpha = \arccos \frac{\nabla c_1 \cdot \nabla c_2}{|\nabla c_1||\nabla c_2|} \tag{14}$$

The synergy angle α reflects the synergic relation for the transmembrane anion and cation driven force in the concentration-driven transmembrane ion transportation. Larger α indicates better ion selectivity. The variation of the synergy angle α presents the same trend with the ion selectivity, as shown in Fig. 4. When pH_L < IEP, the α varies very little with pH_H, and when pH_L > IEP, α decreases and then increases with increasing pH_H, and the

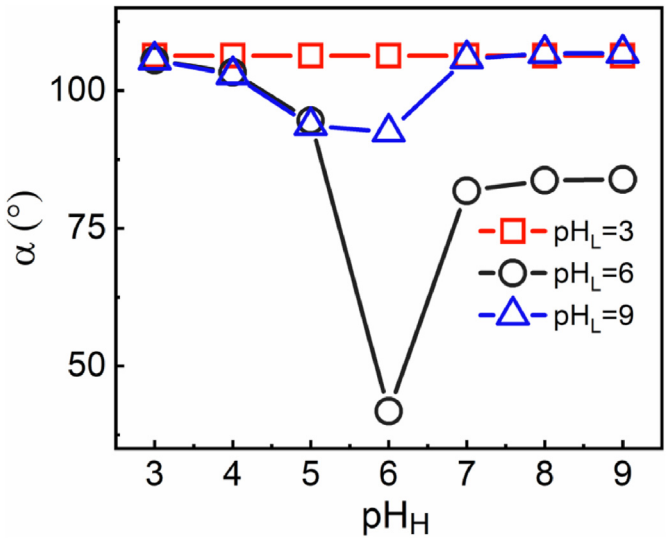

Fig. 4. Impacts of pH at the high concentration side on the synergy angle α

minimum value of α for the latter appears at pH_H = IEP.

The average surface charge density in the nanochannel is shown in Fig. 5(a). When pH_L < IEP, the average surface charge density always remains at a high level and does not change obviously with pH_H. When pH_L>=IEP, the average surface charge density, gradually changes from positive to negative values with increasing pH_H. When pH_L = IEP, the absolute value of the average surface charge density at alkaline is relatively small, while the average surface charge density curve of the system with pH_L = 9 is nearly symmetric about IEP, presenting the same absolute value of surface charge density in acidic and alkaline environments at the same pH interval from the IEP. As shown in Fig. 5 (c), for the studied pH configurations, the surface charge density at the low concentration side is all close to 0, while the surface charge density at the high concentration side is positive when pH_H < IEP and negative when pH_H > IEP. The surface charge density is maximum at the high concentration ends of the nanochannel and minimum at the low concentration ends. The absolute value of the surface charge density at the nanochannel end is significantly higher when pH_H < IEP, rendering better ion selectivity.

To verify the importance of the surface charge density at the low concentration end on the ion selectivity, we calculated the average value for a section of 100 nm length near the low concentration end, as depicted in Fig. 5(b). When the pH of the low concentration end is 3, the surface charge density at the end of the channel changed very small. When the pH of the low concentration is 6, the average surface charge density decreases with increasing pH_H and reaches the minimum value after pH_H>=IEP, which leads to the vanished ion selectivity. When the pH at the low concentration side is 9, the surface charge density near the channel end gradually changes from positive to negative values as the pH_H increases from 3 to 9, which is consistent with the phenomenon of ion selectivity revealed in Fig. 3. At pH_L = 9, the ion selectivity vanishes when pH_H is located between 4 and 5, due to the absence of the surface charge density.

The osmotic current, membrane potential, maximum output electric power, and maximum power efficiency η_{max} under different pH_H are shown in Fig. 6. At pH_L < IEP (pHL = 3), the osmotic current, membrane potential, maximum output electric

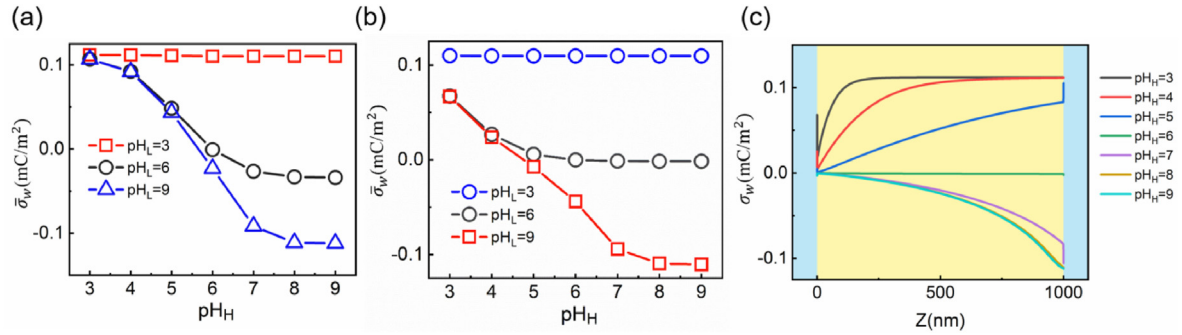

Fig. 5. (a) Effect of pH_H on the average surface charge density over the full length of the channel. (b) Effect of pH_H on the average surface charge density for a section of 100 nm length near the low concentration end. (c) The axial surface charge density of the channel at $pH_L = 6$.

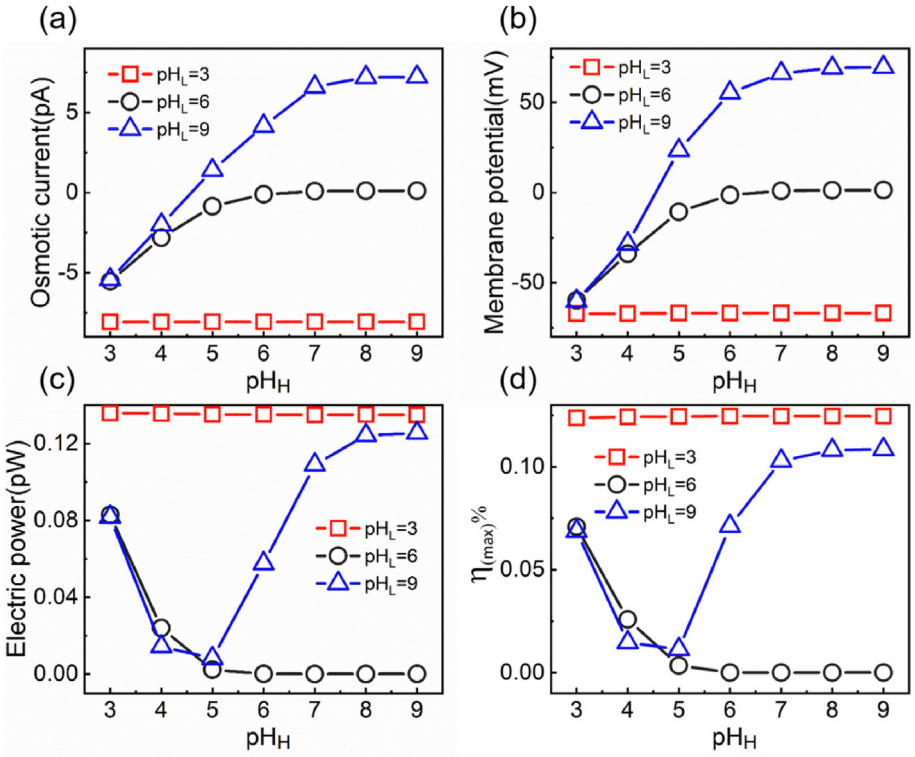

Fig. 6. Impacts of pH at the high concentration side on (a) osmotic current, (b) membrane potential, (c) maximum output power, (d) efficiency at maximum output power.

power, and maximum power efficiency nearly do not vary with pH_H due to invariant surface charge density. In this case, the system presents the highest electric power and energy efficiency among all the studied pH_L. When pH_L > IEP, the osmotic current and membrane potential first decreases with increasing pH_H, reaching its minimum value, then increases. At higher pH_H, the osmotic current and membrane potential reach a plateau and stay stable. When pH_L = IEP, the osmotic current and membrane potential nearly vanish at higher pH_H due to vanished surface charge density. As the osmotic current and membrane potential at pH_L < IEP do not change with varying pH_H, the electric power and energy efficiency also maintain stability under any pH_H, as shown in Fig. 6 (c) and Fig. 6 (d). When pH_L = IEP, due to vanished osmotic current and membrane potential at higher pH_H, the electric power and energy efficiency decrease gradually with increasing pH_H. At higher pH_H, the system has no significant output power and energy conversion efficiency. When pH_L > IEP, the electric power and energy efficiency first decrease with increasing pHH, reach their minimum value, then increase. At higher pH_H, the electric power and energy efficiency reach their maximum values and stay stable.

3.3. Impacts of the solution pH at the low concentration side

Here the impacts of the solution pH at the low concentration side on the energy conversion performance are systematically investigated. The pH at the low concentration side of the nanochannel varies from pH = 3 to pH = 9 with the pH on the high concentration side fixed at different values. The relation of the cation transference number and pH_L under various pH_H is shown in Fig. 7. When pH_H = 3, the ion selectivity decreases slightly with

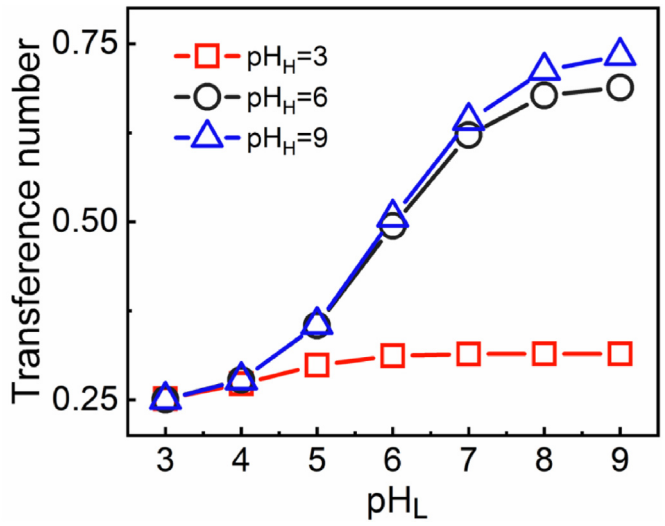

Fig. 7. The relation of the cation transference number and pH_L under various pH_H.

increasing pH_L in the interval of pH_L<=IEP, and the cation transference number remains constant after pH_L > IEP. The system has the highest ion selectivity at $pH_L = 3$. When pH_H > IEP, the ion selectivity of the system first decreases, reaches its minimum value, and then increases as pH_L increases. The lowest value of ion selectivity occurs at pH_L = IEP where the ion selectivity vanishes. At small pH_L, the cation transference number for $pH_H = 6$ (IEP) and $pH_H = 9$ (alkaline) is very close to each other. At higher pH_L, the ion selectivity at $pH_H = 9$ is slightly larger than that at $pH_H = 6$.

As shown in Fig. 8, when pH_H < IEP, the synergy angle α varies very little at various pH_H. When pH_H>=IEP, as pH_H increases, α first decreases, reaches the minimum value of α at pH_H = IEP, and then increases. When pH_L < IEP, the nanochannel has the same value of synergy angle under pH_H = IEP and $pH_H = 9$, which are following the variation of the ion selectivity, as shown in Fig. 8.

The average surface charge density of the whole nanochannel is shown in Fig. 9(a). When $pH_H = 3$, the average charge density for a section of 100 nm length near the low concentration end shows a little decrease with pH_L increasing from 3 to IEP. When $pH_H = 9$, the

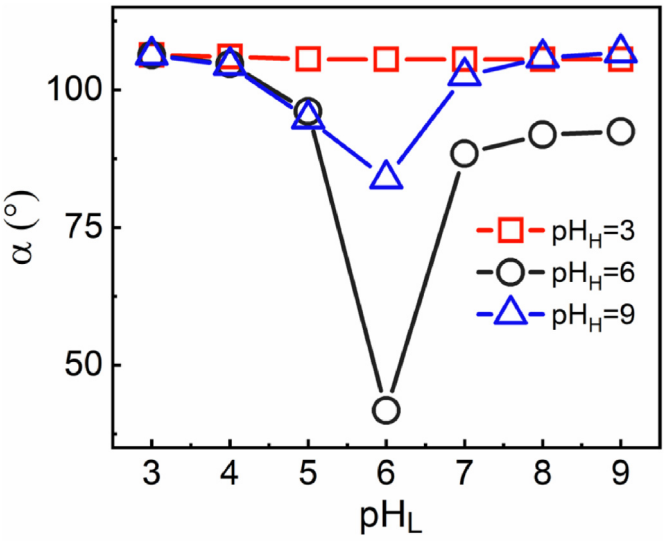

Fig. 8. Impacts of pH at the low concentration side on the synergy angle α

average charge density near the nanochannel end changes from 0.1 mC/m^2 to −0.1 mC/m^2, presenting the same absolute value of σ at the same pH interval from the IEP, which is consistent with the phenomenon of ion selectivity revealed in Fig. 7. As shown in Fig. 9 (c), when pH_L = IEP, for the studied pH configurations, the surface charge density at the low concentration side is smaller than that at the high concentration side. The surface charge density of the nanochannel varies obviously with the pH_L changing from 3 to 9. When pH_L < IEP, the surface charge density is always positive along the channel length. And when pH_L > IEP, the surface charge density stays negative.

The osmotic current I_{osm}, membrane potential E_{diff}, maximum output electric power P_{max}, and maximum power efficiency η_{max} under different pHH are shown in Fig. 10. When pHH<=IEP (pHH = 3), the osmotic current and membrane potential first decrease with the increasing of the pH at the low concentration end and then reaches a stable value after the pHL > IEP. When pHH>=IEP, the osmotic current and membrane potential decrease first and reaches the minimum value at pHL = IEP, and then increases at higher pHL. When pHL < IEP, the electric power and energy efficiency at pHH = 6 and pHH = 9 coincide with each other. Based on the directions of the transmembrane concentration gradient and the pH gradient, the system takes form in two configurations. the co-direction configuration where the transmembrane salinity gradient is in the same direction with the pH gradient, and the reverse direction configuration where the transmembrane salinity gradient is in the opposite direction with the pH gradient. The performance of salinity gradient power generation can be easily improved by regulating the pH of the nanochannel, due to the pH depended on surface charge density distribution, as shown in Fig. 9. In the co-direction configuration, such as pHH = 9 and pHL = 3, electric power and energy efficiency are larger than those under the reverse direction configuration, such as pHH = 3 and pHL = 9.

3.4. Impacts of pH gradient under various nanochannel lengths

Here the impacts of pH gradient under various nanochannel lengths on the energy conversion performance are investigated. The length varies from 50 nm to 2000 nm. In the aforementioned study, under the co-direction configuration, the system exhibits a higher output electric power than that under the reverse direction configuration where the transmembrane salinity gradient is in the opposite direction with the pH gradient. Here the performance under different channel lengths in the co-direction configuration and reverse direction configuration is investigated. Here, nanochannel length varies from 50 nm to 2000 nm. In the co-direction configuration, $pH_H = 9$ and $pH_L = 3$. In the reverse direction configuration, $pH_H = 3$ and $pH_L = 9$.

The cation transference number t_+, osmotic current I_{osm}, membrane potential E_{diff}, maximum output electric power P_{max}, and maximum power efficiency η_{max} under various nanochannel lengths are shown in Fig. 11 and Fig. 12 Osmotic current decreases due to weakened transmembrane concentration gradient, as the nanochannel length varies from 50 nm to 2000 nm. Longer nanochannels have a better ion selectivity and thus higher membrane potential, due to improved EDL overlapping degree. Since the osmotic current and membrane potential have opposite trends, the maximum output electric power first increases, reaches the maximum value and then decreases with increasing length nanochannel.

In the co-direction configuration, the maximum electric power occurs under the situation of the length nanochannel at 300 nm. In the reverse direction configuration, the maximum electric power is located at the 200 nm length nanochannel. Longer nanochannel

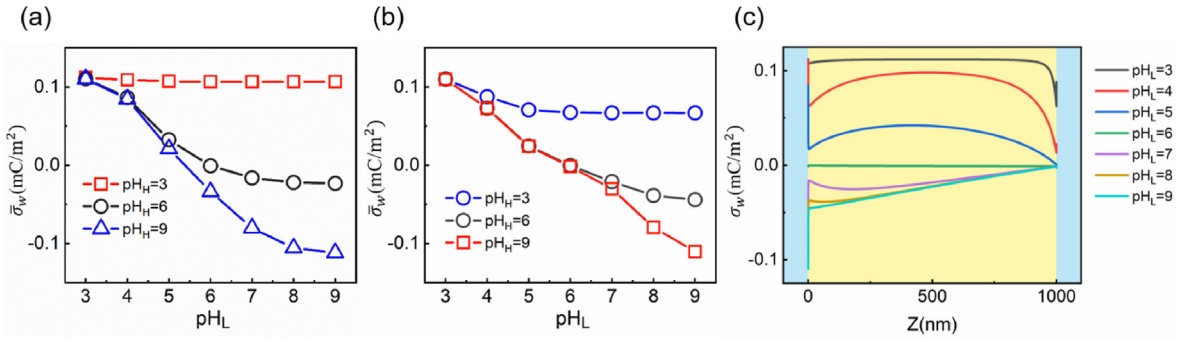

Fig. 9. (a) Effect of pHL on the average surface charge density over the full length of the channel. (b) Effect of pHL on the average surface charge density for a section of 100 nm length near the low concentration end. (c) The axial surface charge density of the channel at pHH = 6.

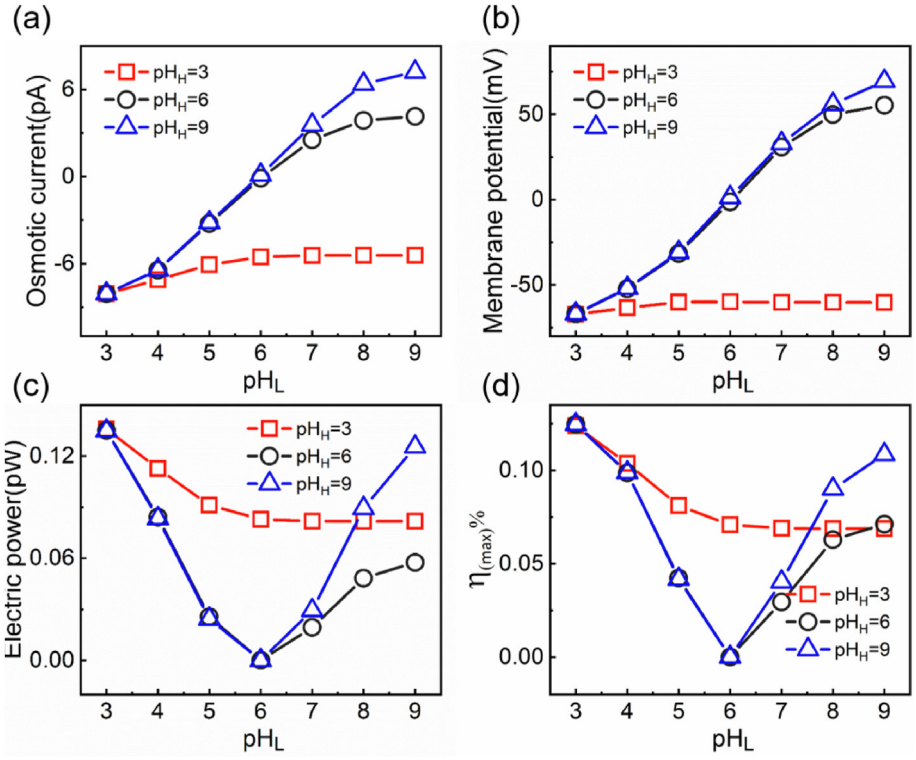

Fig. 10. Impacts of pH at low concentration side on (a) osmotic current, (b) membrane potential, (c) maximum output power, (d) efficiency at maximum output power under different pH$_H$.

has a higher efficiency of the max output power due to improved ion selectivity and weakened ion concentration polarization. For any channel length, the osmotic current, membrane potential, electric power, and energy efficiency in the co-direction configuration are larger than those in the reverse direction configuration. The ratio between the performance indicator in the co-direction configuration and that in the reverse direction configuration is denoted as relative difference (RD), as shown in Fig. 11. The relative difference of ion selectivity increases with the channel length increasing and reaches 40% when the nanochannel length is 2000 nm. The relative difference of osmotic current also expanded with the increasing channel length, and osmotic current in the co-direction configuration is 65.1% higher than that in the reverse direction configuration at a length of 2000 nm. The relative difference of membrane potential is relatively small, which first increases with increasing channel length and then decreases. The maximum relative difference occurs at 1000 nm, with a maximum value of 10.9%. The relative difference of the max output electric power and electric efficiency also augments with increasing length, which reaches 78% and 97.9% at a length of 2000 nm, respectively.

The total ion concentration $C_{total} = \sum_{j=1}^{4} C_j(z)$ at the low concentration end is shown in Fig. 13. The ion concentration polarization phenomenon (ICP) in the short channel is obvious, and the effective concentration ratio in the channel is smaller than the bulk concentration ratio. The obvious ICP leads to increased ion concentration near the short nanochannel end while the total ion concentration is close to the bulk concentration in the long nanochannel. The electric double layer (EDL) overlap degree is weakened as large total ion concentration at the short nanochannel, which results in lowered ion selectivity. As depicted in Fig. 14, at long channel length, the ion separation is more obvious, rendering

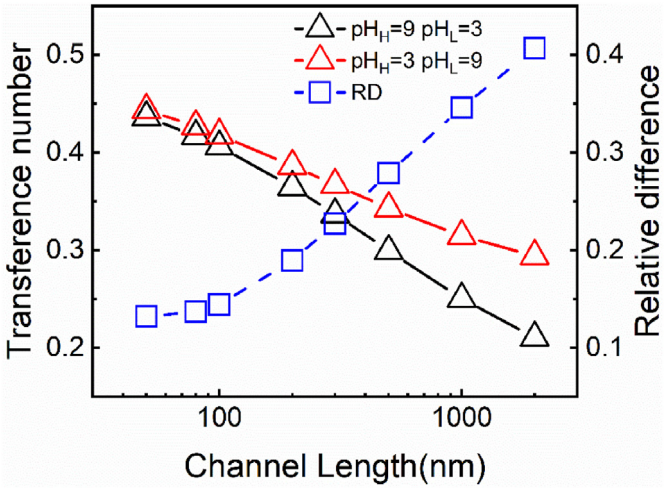

Fig. 11. Impacts of channel length on cation transference number in the co-direction configuration and reverse direction configuration.

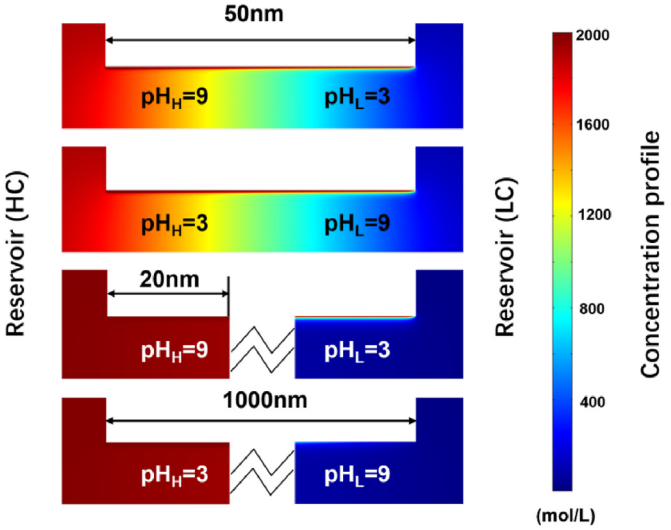

Fig. 13. Total ion concentration distribution for long and short nanochannels. The ICP phenomenon is significant in the short nanochannel and is weakened in the long nanochannel.

higher ion selectivity. Moreover, the ion separation in the co-direction configuration is more significant than that in the reverse direction configuration. The surface charge density for a section of 20 nm length near the low concentration end is shown in Fig. 14(c), (d). The surface charge densities in the co-direction configuration and the reverse direction configuration do not exhibit obvious differences for short nanochannel. However, they differ obviously for long nanochannel. The higher surface charge density in the co-direction configuration leads to a better EDL overlap degree, which contributes to a higher ion selectivity of long nanochannel, and a larger relative difference of the electric power and energy efficiency.

4. Conclusion

Here the impacts of transmembrane pH gradients on nanofluidic salinity gradient energy conversion are systematically investigated via the performance indicators such as cation transference number, osmotic current, membrane potential, maximum output power, and the corresponding energy conversion efficiency.

1. The solution pH at the low concentration side (pH_L) exhibits a significant impact on the energy acquisition ability of the

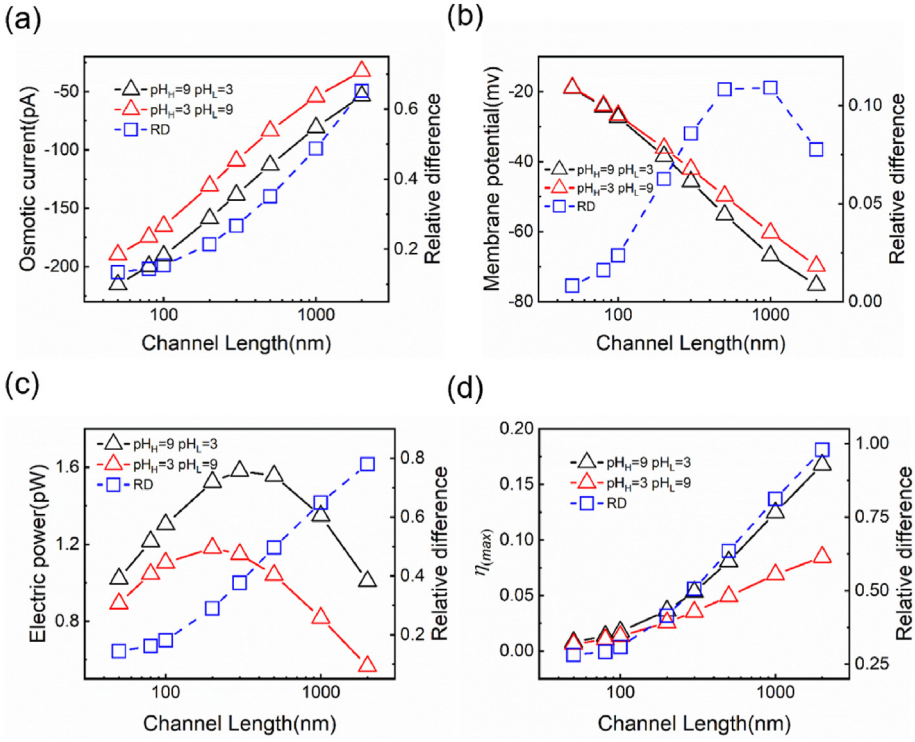

Fig. 12. Impacts of channel length on (a) osmotic current, (b)membrane potential, (c)maximum output power, (d)maximum output power efficiency in the co-direction configuration and reverse direction configuration.

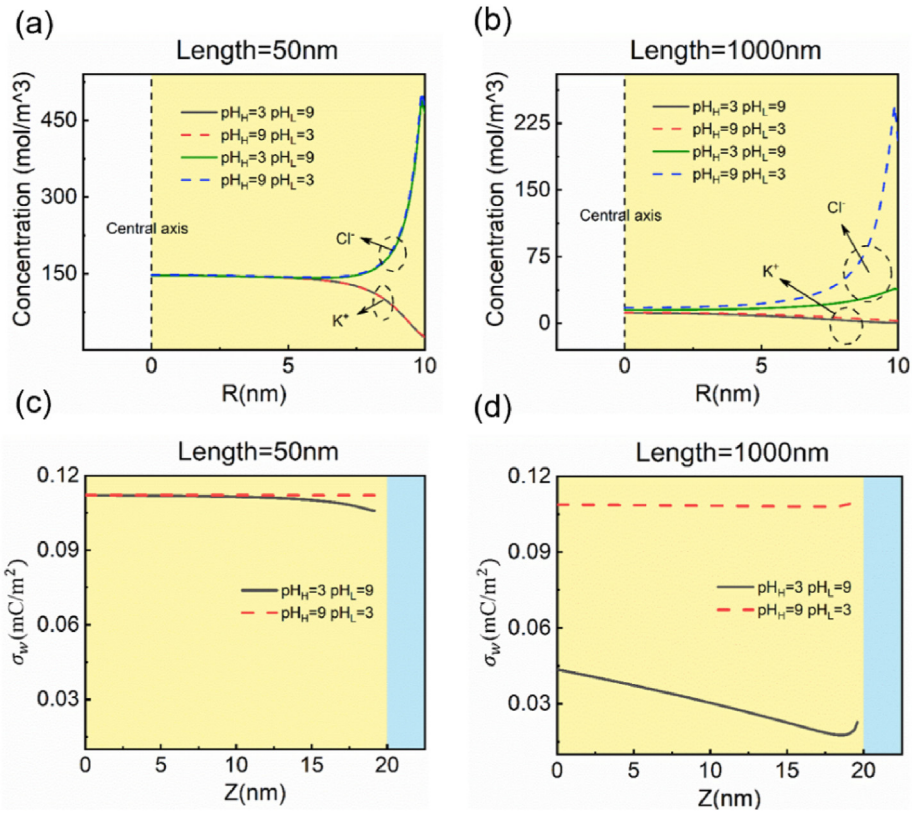

Fig. 14. (a, b) Radial ion concentration at the low concentration end for short and long nanochannels. (c, d) Surface charge density section of 20 nm length near the low concentration end for short and long nanochannels.

salinity gradient energy conversion. The surface charge density of the nanochannel at the low concentration side dominates the nanochannel performance, where the solution pH nanochannel plays a regulatory role. When pH_L < IEP, the energy conversion performance is most stable under various solution pH at the high concentration side (pH_H).

2. Under the co-direction configuration, the system exhibits a higher output electric power than that under the reverse direction configuration where the transmembrane salinity gradient is in the opposite direction with the pH gradient.
3. There exists optimal nanochannel length to maximize the electric power, which differs under various pH configurations. In the co-direction configuration, the maximum electric power occurs under the situation of the length nanochannel at 300 nm. In the reverse direction configuration, the maximum electric power is located around the 200 nm length nanochannel.
4. For longer nanochannels, the ion concentration polarization effect is weakened, allowing for a more effective energy extraction performance via pH-adjusted salinity gradients. At the length of 2000 nm, the power and efficiency under the co-direction configuration are increased by 78% and 97.9%, respectively, over the nanochannel under the reverse direction configuration.

This study may provide new insights into the pH-regulation nanofluidic salinity-gradient energy harvesting. The conclusions could be used to improve the performance of existing RED devices at a lower cost or provide new ideas for new pH regulation RED designing.

CRediT authorship contribution statement

Xi Chen: Writing – original draft, Visualization. **Zuoqing Luo:** Formal analysis. **Rui Long:** Methodology, Writing – review & editing, Funding acquisition. **Zhichun Liu:** Conceptualization. **Wei Liu:** Formal analysis, Funding acquisition.

Declaration of competing interest

The authors declare that they have no known competing financial interests or personal relationships that could have appeared to influence the work reported in this paper.

Acknowledgments

This work is financially supported by the National Natural Science Foundation of China (52176070, 51736004).

References

[1] M. Habibi Matin, Electroviscous effects on thermal transport of electrolytes in pressure driven flow through nanoslit, Int. J. Heat Mass Tran. 106 (2017) 473–481.
[2] C. Li, Z. Liu, X. Liu, Z. Feng, X. Mo, Combined effect of surface charge and boundary slip on pressure-driven flow and convective heat transfer in nanochannels with overlapping electric double layer, Int. J. Heat Mass Tran. 176 (2021) 121353.
[3] Z.-Q. Li, Z.-Q. Wu, X.-L. Ding, M.-Y. Wu, X.-H. Xia, A solar thermoelectric nanofluidic device for solar thermal energy harvesting, CCS Chem. 3 (7) (2021) 2174–2182.
[4] R. Long, F. Wu, X. Chen, Z. Liu, W. Liu, Temperature-depended ion concentration polarization in electrokinetic energy conversion, Int. J. Heat Mass Tran. 168 (2021) 120842.

[5] R. Long, M. Li, X. Chen, Z. Liu, W. Liu, Synergy analysis for ion selectivity in nanofluidic salinity gradient energy harvesting, Int. J. Heat Mass Tran. 171 (2021) 121126.
[6] Z. Jia, B. Wang, S. Song, Y. Fan, Blue energy: current technologies for sustainable power generation from water salinity gradient, Renew. Sustain. Energy Rev. 31 (2014) 91–100.
[7] O.A. Alvarez-Silva, A.F. Osorio, C. Winter, Practical global salinity gradient energy potential, Renew. Sustain. Energy Rev. 60 (2016) 1387–1395.
[8] R. Long, Z. Kuang, Z. Liu, W. Liu, Reverse electrodialysis in bilayer nanochannels: salinity gradient-driven power generation, Phys. Chem. Chem. Phys. 20 (10) (2018) 7295–7302.
[9] T.W. Lin, J.P. Hsu, Pressure-driven energy conversion of conical nanochannels: anomalous dependence of power generated and efficiency on pH, J. Colloid Interface Sci. 564 (2020) 491–498.
[10] S.A. Shah, S.-Y. Choi, S. Cho, M. Shahbabaei, R. Singh, D. Kim, Modified single-wall carbon nanotube for reducing fouling in perfluorinated membrane-based reverse electrodialysis, Int. J. Hydrogen Energy 45 (55) (2020) 30703–30719.
[11] R. Long, B. Li, Z. Liu, W. Liu, Hybrid membrane distillation-reverse electrodialysis electricity generation system to harvest low-grade thermal energy, J. Membr. Sci. 525 (2017) 107–115.
[12] N.Y. Yip, D.A. Vermaas, K. Nijmeijer, M. Elimelech, Thermodynamic, energy efficiency, and power density analysis of reverse electrodialysis power generation with natural salinity gradients, Environ. Sci. Technol. 48 (9) (2014) 4925–4936.
[13] Y. Tian, D. Li, G. Liu, C. Li, J. Liu, J. Wu, J. Liu, Y. Feng, Formate production from CO2 electroreduction in a salinity-gradient energy intensified microbial electrochemical system, Bioresour. Technol. 320 (2021) 124292.
[14] A. Sepehri, M.-H. Sarrafzadeh, Effect of nitrifiers community on fouling mitigation and nitrification efficiency in a membrane bioreactor, Chem. Eng. Proces. Process Intensif. 128 (2018) 10–18.
[15] F.E. Ahmed, R. Hashaikeh, N. Hilal, Hybrid technologies: the future of energy efficient desalination – a review, Desalination 495 (2020) 114659.
[16] C. Tristán, M. Fallanza, R. Ibáñez, I. Ortiz, Recovery of salinity gradient energy in desalination plants by reverse electrodialysis, Desalination 496 (2020) 114699.
[17] I.E. Mokhtar, L. Gurreri, A. Tamburini, A. Cipollina, M. Ciofalo, S.a.T. Bouguecha, G. Micale, CFD prediction of flow, heat and mass transfer in woven spacer-filled channels for membrane processes, Int. J. Heat Mass Tran. 173 (2021) 121246.
[18] R. Long, Z. Luo, Z. Kuang, Z. Liu, W. Liu, Effects of heat transfer and the membrane thermal conductivity on the thermally nanofluidic salinity gradient energy conversion, Nano Energy 67 (2020) 104284.
[19] A. Siria, P. Poncharal, A.L. Biance, R. Fulcrand, X. Blase, S.T. Purcell, L. Bocquet, Giant osmotic energy conversion measured in a single transmembrane boron nitride nanotube, Nature 494 (7438) (2013) 455–458.
[20] D.-K. Kim, C. Duan, Y.-F. Chen, A. Majumdar, Power generation from concentration gradient by reverse electrodialysis in ion-selective nanochannels, Microfluid. Nanofluidics 9 (6) (2010) 1215–1224.
[21] B.D. Kang, H.J. Kim, M.G. Lee, D.-K. Kim, Numerical study on energy harvesting from concentration gradient by reverse electrodialysis in anodic alumina nanopores, Energy 86 (2015) 525–538.
[22] J. Feng, M. Graf, K. Liu, D. Ovchinnikov, D. Dumcenco, M. Heiranian, V. Nandigana, N.R. Aluru, A. Kis, A. Radenovic, Single-layer MoS2 nanopores as nanopower generators, Nature 536 (7615) (2016) 197–200.
[23] J. Gao, W. Guo, D. Feng, H. Wang, D. Zhao, L. Jiang, High-performance ionic diode membrane for salinity gradient power generation, J. Am. Chem. Soc. 136 (35) (2014) 12265–12272.
[24] T.-W. Lin, J.-P. Hsu, C.-Y. Lin, S. Tseng, Dual pH gradient and voltage modulation of ion transport and current rectification in biomimetic nanopores functionalized with a pH-tunable polyelectrolyte, J. Phys. Chem. C 123 (19) (2019) 12437–12443.
[25] J.-P. Hsu, S.-T. Yang, C.-Y. Lin, S. Tseng, Ionic current rectification in a conical nanopore: influences of electroosmotic flow and type of salt, J. Phys. Chem. C 121 (8) (2017) 4576–4582.
[26] J.-P. Hsu, T.-W. Lin, C.-Y. Lin, S. Tseng, Salt-dependent ion current rectification in conical nanopores: impact of salt concentration and cone angle, J. Phys. Chem. C 121 (50) (2017) 28139–28147.
[27] C. Kubeil, A. Bund, The role of nanopore geometry for the rectification of ionic currents, J. Phys. Chem. C 115 (16) (2011) 7866–7873.
[28] J.-P. Hsu, Y.-C. Chen, Y.-M. Chen, S. Tseng, Influence of temperature and electroosmotic flow on the rectification behavior of conical nanochannels, J. Taiwan Inst. Chem. Eng. 93 (2018) 142–149.
[29] R. Long, F. Wu, X. Chen, Z. Liu, W. Liu, Temperature-depended ion concentration polarization in electrokinetic energy conversion, Int. J. Heat Mass Tran. 168 (2021).
[30] H.-C. Yeh, C.-C. Chang, R.-J. Yang, Reverse electrodialysis in conical-shaped nanopores: salinity gradient-driven power generation, RSC Adv. 4 (6) (2014) 2705–2714.
[31] Z. Kuang, D. Zhang, Y. Shen, R. Long, Z. Liu, W. Liu, Bioinspired fractal nanochannels for high-performance salinity gradient energy conversion, J. Power Sources 418 (2019) 33–41.
[32] A. Esfandiar, B. Radha, F. Wang, Q. Yang, S. Hu, S. Garaj, R.R. Nair, A. Geim, K. Gopinadhan, Size effect in ion transport through angstrom-scale slits, Science 358 (6362) (2017) 511–513.
[33] R. Long, Y. Zhao, Z. Kuang, Z. Liu, W. Liu, Hydrodynamic slip enhanced nanofluidic reverse electrodialysis for salinity gradient energy harvesting, Desalination 477 (2020) 114263.
[34] R. Long, Z. Kuang, Z. Liu, W. Liu, Reverse electrodialysis in bilayer nanochannels: salinity gradient-driven power generation, Phys. Chem. Chem. Phys. 20 (2018) 7295–7302.
[35] Y. Ma, L.H. Yeh, C.Y. Lin, L. Mei, S. Qian, pH-regulated ionic conductance in a nanochannel with overlapped electric double layers, Anal. Chem. 87 (8) (2015) 4508–4514.
[36] S. Tseng, Y.M. Li, C.Y. Lin, J.P. Hsu, Salinity gradient power: influences of temperature and nanopore size, Nanoscale 8 (4) (2016) 2350–2357.
[37] R. Long, Z. Kuang, Z. Liu, W. Liu, Temperature regulated reverse electrodialysis in charged nanopores, J. Membr. Sci. 561 (2018) 1–9.
[38] R. Long, Z. Kuang, Z. Liu, W. Liu, Ionic thermal up-diffusion in nanofluidic salinity-gradient energy harvesting, Natl. Sci. Rev. 6 (6) (2019) 1266–1273.
[39] Y. Peng, T. Zhou, T. Li, L. Shi, L. Wen, The polarization reverse of diode-like conical nanopore under pH gradient, SN Appl. Sci. 2 (11) (2020).
[40] V.-P. Mai, R.-J. Yang, Active control of salinity-based power generation in nanopores using thermal and pH effects, RSC Adv. 10 (32) (2020) 18624–18631.
[41] J.-P. Hsu, S.-C. Lin, C.-Y. Lin, S. Tseng, Power generation by a pH-regulated conical nanopore through reverse electrodialysis, J. Power Sources 366 (2017) 169–177.
[42] L.H. Yeh, F. Chen, Y.T. Chiou, Y.S. Su, Anomalous pH-dependent nanofluidic salinity gradient power, Small 13 (48) (2017) 1702691.
[43] W. Guo, L. Cao, J. Xia, F.-Q. Nie, W. Ma, J. Xue, Y. Song, D. Zhu, Y. Wang, L. Jiang, Energy harvesting with single-ion-selective nanopores: a concentration-gradient-driven nanofluidic power source, Adv. Funct. Mater. 20 (8) (2010) 1339–1344.
[44] S. Tseng, Y.R. Hsu, J.P. Hsu, Diffusiophoresis of polyelectrolytes: effects of temperature, pH, type of ionic species and bulk concentration, J. Colloid Interface Sci. 459 (2015) 167–174.
[45] A.M. Benneker, H.D. Wendt, R.G.H. Lammertink, J.A. Wood, Influence of temperature gradients on charge transport in asymmetric nanochannels, Phys. Chem. Chem. Phys. 19 (41) (2017) 28232–28238.
[46] J.A. Wood, A.M. Benneker, R.G. Lammertink, Temperature effects on the electrohydrodynamic and electrokinetic behaviour of ion-selective nanochannels, J. Phys. Condens. Matter 28 (11) (2016) 114002.